

Persistent-homology-based gait recognition*

J. Lamar-Leon, Raul Alonso-Baryolo , Edel Garcia-Reyes
 Advance Technologies Application Center (CENATAV), La Habana, Cuba
 {jlamar,rbaryolo,egarcia}@cenatav.co.cu

R. Gonzalez-Diaz
 Applied Math Dept. I, IMUS, Universidad de Sevilla, Spain
 rogo@us.es

Abstract

Gait recognition is an important biometric technique for video surveillance tasks, due to the advantage of using it at distance. In this paper, we present a persistent homology-based method to extract topological features (the so-called *topological gait signature*) from the body silhouettes of a gait sequence. It has been used before in several conference papers of the same authors for human identification, gender classification, carried object detection and monitoring human activities at distance. The novelty of this paper is the study of the stability of the topological gait signature under small perturbations and the number of gait cycles contained in a gait sequence. In other words, we show that the topological gait signature is robust to the presence of noise in the body silhouettes and to the number of gait cycles contained in a given gait sequence. We also show that computing our topological gait signature of only the lowest fourth part of the body silhouette, we avoid the upper body movements that are unrelated to the natural dynamic of the gait, caused for example by carrying a bag or wearing a coat.

Keywords: Feature extraction, Gait recognition, Video sequences, Persistent Homology,

1 Introduction

Persons recognition at distance, without the subject cooperation, is an important task in video surveillance. Very few biometric techniques can be used in these scenarios. Gait recognition is a technique with special potential under these circumstances due to its advantages, since the features can be extracted from any viewpoint and at bigger distances than other biometric approaches.

*Partially supported by MINECO/FEDER-UE under grant MTM2015-67072-P. General acknowledgments should be placed at the end of the article.

Currently, there are good results in the state of the art for persons walking under natural conditions (without carrying a bag or wearing a coat). See, for example, [17, 11, 10]. However, it is not common for people to walk without carrying a bag or anything that changes the natural gait. Moreover, people usually perform movements with the upper body part unrelated to the natural dynamic of the gait. Up to now, the most successful approaches in gait recognition use silhouettes to get the features. Among the silhouette-based techniques, the best results have been obtained from the methods based in Gait Energy Images (GEI) [18, 17, 11, 14, 16]. Besides, the GEI methods have been used to eliminate the effects of carrying a bag or wearing a coat in [1, 11, 17]. Generally, these strategies are affected by a small number of silhouettes (one gait cycle or less). Moreover, the temporal order in which silhouettes appear is not captured in those representations, losing the relative relations of the movements in time. Besides, the features extracted by these methods are highly correlated with errors in the segmentation of the silhouettes [3] and these errors frequently appear in the existing algorithms for background segmentation. This implies that GEI methods are influenced by the shape of the silhouette instead of the relative positions among the parts of the body while walking. The accuracy in gait recognition for persons carrying bag or using coat can be consulted in [17] for the CASIA-B gait dataset¹. The authors in [17] used features from the full body but the results were not satisfactory. For instance, the best result for persons walking with coats was 32.7% using lateral view, while the worst result was 24.6%, using frontal view. Besides, for persons carrying a bag, the best result was 80.2% using frontal view and the worst 52.0%, using lateral view.

In our conference papers [10, 9, 6, 7], we concentrated our effort in overcoming most of the difficulties explained above, which took us to get promising results. In those works, the gait was modeled using a persistent-homology-based representation (called topological signature of the gait sequence), since it gives features of the objects that are invariant to deformation. The topological signature of the gait sequence was used for human identification in [10], gender classification in [9], carried object detection in [6] and monitoring human activities at distance in [7]. Later, in [8], we applied our persistent-homology-based gait recognition method using only the lower part of the body, i.e., the legs (see Fig. 1), avoiding many of the effects arising from the variability in the upper body part.

In this paper, we first recall our persistent-homology-based method for gait recognition in order to be self-contained. The input of the procedure is a sequence of human silhouettes obtained from a video. A simplicial complex $\partial K(I)$ which represents the human gait is then constructed (see Section 2). Sixteen persistence barcodes (a known tool in the Theory of Persistent

¹<http://www.cbsr.ia.ac.cn/GaitDatasetB-silh.zip>

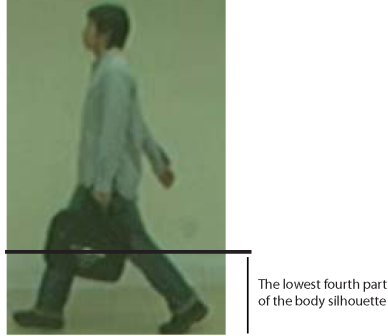


Figure 1: Lowest four part of the body occluded by a bag.

Homology) are then computed (see Section 3) considering, respectively, the distance to eight fixed planes (2 horizontal, 2 vertical, 2 oblique and 2 depth planes) in order to completely capture the movement in the gait sequence. More concretely, for each plane π , we compute two persistence barcodes: one to detect the variation of connected components and the other to detect the variation of tunnels when we go through $\partial K(I)$ in a direction perpendicular to the plane π . Putting together all this information, we construct a vector (called topological signature) associated to each gait sequence. To compare two topological signatures, we use the angle between both vectors. To decrease the negative effects of variations unrelated to the gait in the upper body part, we can only select the lowest fourth part of the body silhouette (legs-silhouette) (as we did in [8]). As a contribution of this paper, we study the stability of the topological signature in Section 4. We prove, in terms of probabilities, that small perturbations in the input body silhouettes provoke small perturbations in the resulting topological signature. We also show that the direction of the topological signature (which is a vector) of a gait sequence remains the same independently on the number of gait cycles it contains. To compare two topological signatures, we use the angle between the corresponding vectors, then the previous assertion implies that the topological signature is independent on the number of gait cycles the gait sequence contains. Experimental results are showed in Section 5 and are analyzed in Section 6. Conclusions are finally given in Section 7.

2 Topological model of the gait: Simplicial Complexes

In this section we introduce the construction of the simplicial complex $\partial K(I)$ which represents the input human gait sequence.

We start the procedure with a sequence of silhouettes obtained from a gait sequence. With the intention of a fair comparison, we get the sequences

from the background segmentation provided in CASIA-B dataset². See Fig. 2.Left.

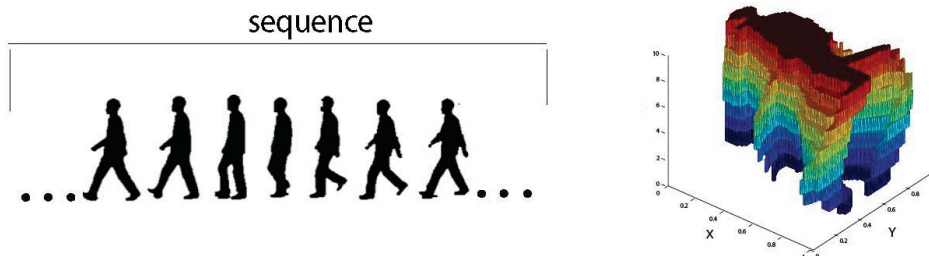


Figure 2: Left: Sequence of gait silhouettes. Right: Simplicial complex $\partial K(I)$.

We then build a 3D binary image $I = (\mathbb{Z}^3, B)$ by stacking k consecutive silhouettes. Recall that a *3D binary image* is a pair $I = (\mathbb{Z}^3, B)$, where B (called the *foreground*) is a **finite** subset of \mathbb{Z}^3 and $B^c = \mathbb{Z}^3 \setminus B$ is the *background*. Later, $I = (\mathbb{Z}^3, B)$ is used to derive a cubical complex $Q(I)$. The *cubical complex* $Q(I)$ is a combinatorial structure constituted by a set of unit cubes with faces parallel to the coordinate planes and vertices in \mathbb{Z}^3 , together with all its faces. The *0-faces* of a cube c are its 8 corners (vertices), its *1-faces* are its 12 edges, its *2-faces* are its 6 squares and, finally, its *3-face* is the cube itself. Then, a cube with vertices $V = \{(i, j, k), (i+1, j, k), (i, j+1, k), (i+1, j+1, k), (i, j, k+1), (i+1, j, k+1), (i, j+1, k+1), (i+1, j+1, k+1)\}$, with $(i, j, k) \in \mathbb{Z}^3$, is added to $Q(I)$ together with all its faces if and only if $V \subseteq B$. Finally, the squares that are faces of exactly one cube in $Q(I)$ are divided into two triangles. These triangles together with their faces (vertices and edges) form the *simplicial complex* $\partial K(I)$. See Fig. 2.Right. The formal definition of a simplicial complex K is as follows [13, p. 7]: A simplicial complex K is a collection of simplices³ in \mathbb{R}^n such that: (1) every face of a simplex of K is in K ; and (2) the intersection of any two simplices of K is a face of each of them. Notice that the height of each silhouette is set to 1 and the width changes accordingly to preserve the original proportion between height and width. z -Coordinates represents the amount of silhouettes in the stack which is not fixed (see Fig. 2.Right).

To decrease the negative effects of variations unrelated to the gait in the upper body part (related, for example, to hand gestures like talking on cell), in [8] we selected the lowest fourth part of the body silhouette (legs-silhouette) (see Fig. 3). This selection is endorsed by the result given in [1], which shows that this part of the body provides most of the necessary information for classification.

²<http://www.cbsr.ia.ac.cn/GaitDatasetB-silh.zip>

³The simplices considered in this paper are 0-simplices (i.e. vertices), 1-simplices (i.e. edges) and 2-simplices (i.e. triangles).

Finally, notice that, in [8] and this paper, not only the height but also the depth is set to 1. This way, from now on in this paper, x -, y - and z -coordinates of the vertices in $\partial K(I)$ have their values in the interval $[0, 1]$ (see Fig. 3.Right).

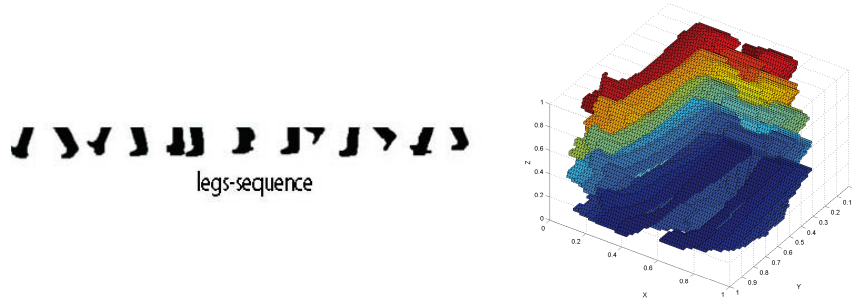


Figure 3: Left: Sequence of legs-silhouettes. Right: Simplicial complex $\partial K(I)$ of a legs-silhouette sequence.

2.1 Filtration of the Simplicial Complex $\partial K(I)$

The next step in our process is to sort the simplices of $\partial K(I)$ in order to obtain a filtration.

A *filtration* is a partial ordering of the simplices of $\partial K(I)$ dictated by a *filter function* $f : \partial K(I) \rightarrow \mathbb{R}$, satisfying that if a simplex σ is a face of another simplex σ' in $\partial K(I)$ then $f(\sigma) \leq f(\sigma')$ (i.e., σ appears before or at the same time that σ' in the ordering).

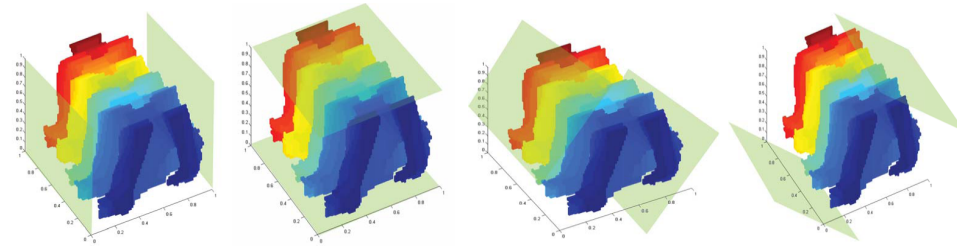


Figure 4: From left to right: The eight planes used for computing the eight filtrations for $\partial K(I)$: two vertical planes, two horizontal planes and four oblique planes.

In our work, we use eight filtrations obtained from eight planes (see Fig. 4). For each plane π , we define the filter function $f_\pi : \partial K(I) \rightarrow \mathbb{R}$ which assigns to each vertex of $\partial K(I)$ its distance to the plane π , and to any other simplex of $\partial K(I)$, the biggest distance of its vertices to π . Ordering the

simplices of $\partial K(I)$ according to the values of f_π , we obtain the filtration ∂K_π for $\partial K(I)$ associated to the plane π .

Notice that, in [10, 9, 6, 7], the filtration associated to each plane π is obtained in a different way: By adding one simplex at each time (i.e., a total ordering of the simplices is constructed). Nevertheless, the filtration presented in [8] and in this paper, is constructed by adding a bunch of simplices at each time (all the simplices of $\partial K(I)$ with same distance to the reference plane π). This way, different times represent sets of simplices with possibly different cardinalities, which makes the method robust to variation in the amount of simplices of the simplicial complex and therefore, robust to noise. Besides, the difficulties we had previously in [10, 9, 6, 7] with the stability of the sorting algorithm disappear in [8] and in this paper, since each set of simplices in the filtration contains all the simplices with the same distance to a reference plane, and these sets are sorted according to their associated distances.

3 Persistent homology and topological signature

The final step in our process to obtain the topological signature of a gait sequence is to compute the persistent homology of each filtration.

Persistent homology is an algebraic tool for measuring topological features of shapes and functions. It is built on top of homology, which is a topological invariant that captures the amount of connected components, tunnels, cavities and higher-dimensional counterparts of a shape. Small size features in persistent homology are often categorized as noise, while large size features describe topological properties of shapes [4].

Formally, let K be a simplicial complex. A p -chain on K is a formal sum of p -simplices of K . The group of p -chains is denoted by $C_p(K)$. Let us define the homomorphism: $\partial_p : C_p(K) \rightarrow C_{p-1}(K)$ called *boundary operator* such that for each p -simplex σ of K , $\partial_p(\sigma)$ is the sum of its faces. For example, if σ is a triangle, $\partial_2(\sigma)$ is the sum of its edges. The kernel of ∂_p is called the group of p -cycles in $C_p(K)$ and the image of ∂_{p+1} is called the group of p -boundaries in $C_p(K)$. The p -homology $H_p(K)$ of K is the quotient group of p -cycles relative to p -boundaries (see [13, Chapter 5]). Then, 0-homology classes (i.e. the classes in $H_0(K)$) represent the connected components of K , 1-homology classes its tunnels and 2-homology classes its cavities.

Now, consider a filtration F for a simplicial complex K obtained from a given filter function $f : K \rightarrow \mathbb{R}$. To simplify the explanation, suppose that the simplices of the filtration are totally ordered (i.e., exactly one simplex is added each time). Let $F = (\sigma_1, \sigma_2, \dots, \sigma_m)$. If σ_i completes a p -cycle (p being the dimension of σ_i) when σ_i is added to $F_{i-1} = (\sigma_1, \dots, \sigma_{i-1})$, then a p -homology class α is born at time $f(\sigma_i)$; otherwise, a $(p-1)$ -homology

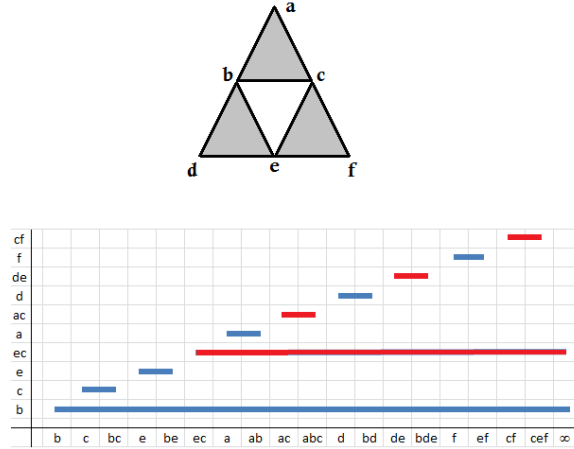


Figure 5: An example of a persistence barcode obtained from a simplicial complex.

class *dies at time* $f(\sigma_i)$. The difference between the birth and death times of a homology class γ is called its *persistence*, which quantifies the significance of a topological attribute. If α never dies, we set its persistence to infinity.

For a p -homology class that is born at time $f(\sigma_i)$ and dies at time $f(\sigma_j)$, we draw a **bar** $[f(\sigma_i), f(\sigma_j))$ with endpoints $f(\sigma_i)$ and $f(\sigma_j)$. The set of bars $\{[f(\sigma_i), f(\sigma_j))\}$ representing birth and death times of homology classes is called the *persistence barcode* $B(F)$ of the filtration F . See, for example, Fig. 6. Analogously, the set of points $\{(f(\sigma_i), f(\sigma_j)) \in \mathbb{R}^2\}$ is called the *persistence diagram* $dgm(F)$ of the filtration F . See, for example, Fig. 8.

For example, in Fig. 5, bars corresponding to the persistence of 0-homology classes (i.e. the persistence of connected components) are colored in blue and bars corresponding to the persistence of 1-homology classes (i.e., the persistence of tunnels) are colored in red. The filtration $F = \{b, c, bc, e, be, ec, a, ab, ac, abc, d, bd, de, bde, f, ef, cf, cef\}$ which, in this case, is a total ordering, can also be read on the x axis of the diagram. Observe that only two bars survive until the end (the one corresponding to the connected component and the other corresponding to the tunnel).

For a detailed introduction on the theoretical concepts introduced above see, for example, [4, 5].

As an example, the persistence barcodes for the video sequences **001-nm-01-090** and **002-nm-01-090** in the CAISA-B dataset are shown in Fig. 6. The red bars represent the persistence of 0-homology classes while the blue ones represent the persistence of 1-homology classes. For computing these barcodes, we used the leftmost plane of Fig. 4. Notice the green circle showing topological features that born and die at the same time.

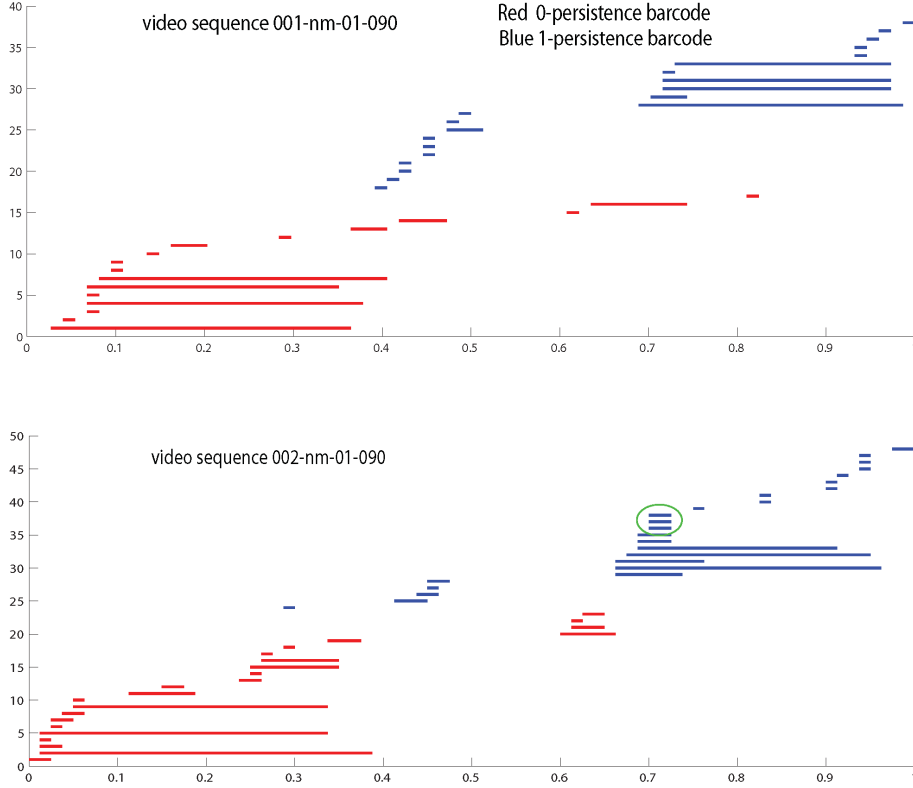


Figure 6: Persistence barcodes for the sequences 001-nm-01-090 and 002-nm-01-090 of CAISA-B dataset. Horizontal axis represents the distance to the reference plane, normalized to $[0,1]$.

3.1 Topological Signature for a Gait Sequence

Now, the topological signature is computed from the persistence barcodes obtained for ∂K_π for each plane π shown in Fig. 4. Observe that fixed a reference plane π , the length of each interval in the persistence barcode obtained for ∂K_π is: (a) less or equal than 1 if π is an horizontal o vertical plane, and (b) less or equal than $\sqrt{2}$ if π is an oblique plane.

For computing the topological signature we only consider bars in the persistence barcode with length strictly greater than 0. This way, we do not take into account any topological event e that is born and dies at the same distance to the reference plane. This is not a problem, since that event e will be capture using a different reference plane.

Now, for computing the *topological signature*, for each plane π , the 0--persistence barcode (i.e., the lifetime of connected components) and the 1--persistence barcode (i.e., the lifetime of tunnels) of the filtration ∂K_π are explored according to a uniform sampling. More concretely, given a positive integer n (being $n = 24$ in our experimental results, obtained by

cross validation), we compute the value $h = \frac{k}{n}$, which represents the width of the “window” we use to analyze the persistence barcode, being k the biggest distance of a vertex in $\partial K(I)$ to the given plane π . Since the distance to the plane has been normalized in order to compute the topological signature, then $k \leq \sqrt{2}$, so $h \leq \frac{\sqrt{2}}{24}$. Then, a vector \mathcal{V}_π^0 (resp. \mathcal{V}_π^1) of $2n$ entries is then constructed as follows:

Procedure 1 For $s = 0, \dots, n - 1$,

- (a) entry $2s$ contains the number of 0– (resp. 1–) homology classes that are born before $s \cdot h$;
- (b) entry $2s + 1$ contains the number of 0– (resp. 1–) homology classes that are born in $s \cdot h$ or later and before $(s + 1) \cdot h$.

Observe that dividing the entries in two categories (a) and (b), small details in the object are highlighted, which is crucial for distinguishing two different gaits. For example, let us suppose an scenario in which m 0–homology classes are born in $[s \cdot h, (s + 1) \cdot h)$ and persist or die at the end of $[(s + 1) \cdot h, (s + 2) \cdot h)$ and not any other 0–homology class is born, persists or dies in these intervals. Then, we put 0 in entries $2s$ and $2s + 3$ of \mathcal{V}_π^0 , and m in entries $2s + 1$ and $2s + 2$ of \mathcal{V}_π^0 . On the other hand, let us suppose that m 0–homology classes are born and die in $[s \cdot h, (s + 1) \cdot h)$ and in $[(s + 1) \cdot h, (s + 2) \cdot h)$ and not any other 0–homology class is born, persists or dies in these intervals. Then, we put 0 in entries $2s$ and $2s + 2$ of \mathcal{V}_π^0 and m in entries $2s + 1$ and $2s + 3$ of \mathcal{V}_π^0 . Observe that only considering (a) and (b) separately, we can distinguish both scenarios.

This way, fixed a plane π , we obtain two $2n$ –dimensional vectors for ∂K_π , one for the 0–persistence barcode and the other for the 1–persistence barcode associated to the filtration ∂K_π . Since we have eight planes, $\{\pi_1, \dots, \pi_8\}$, and two vectors per plane, $\{\mathcal{V}_{\pi_i}^0, \mathcal{V}_{\pi_i}^1\} : i = 1, \dots, 8$, we have a total of sixteen $2n$ –dimensional vectors which form the *topological signature for a gait sequence*.

Finally, for comparing the topological signatures of two gait sequences, we add up the angle between each pair of the corresponding vectors conforming the topological signatures. Since a signature consists of sixteen vectors, the best comparison for two sequences is obtained when the total sum is zero and the worst is $90 \cdot 16 = 1440$. Observe that in our previous papers [10, 9, 6, 7], we used the cosine distance to compare two given topological signatures. We have noticed that using the angle instead of the cosine, the efficiency (accuracy) increases by 5%. This comparison is made in Table 5 in Section 5.

4 Stability of the topological signature for a gait sequence

Once we have defined the *topological signature for a gait sequence*, our aim in this section is to prove its stability under small perturbations on the gait sequence and/or on the number of gait cycles contained in the gait sequence.

First, we introduce some theoretical concepts needed to prove the statements above. The bottleneck distance (see [4, page 229]) is classically used to compare the persistence diagrams of two different filtrations. Concretely, let F and F' be two filtrations of, respectively, two finite simplicial complexes K and K' . Since K and K' are finite then $dgm(F)$ and $dgm(F')$ are finite. Let $dgm(F) = \{a_1, \dots, a_k\}$ and $dgm(F') = \{a'_1, \dots, a'_{k'}\}$ be the persistence diagrams of F and F' , respectively. Then

$$d_b(dgm(F), dgm(F')) = \min_{\gamma} \{ \max_a \{ \|a - \gamma(a)\|_{\infty} \} \}$$

is the *bottleneck distance* between $dgm(F)$ and $dgm(F')$ where, for points $a = (x, y) \in F \cup D$ and $\gamma(a) = (x', y') \in F' \cup D$ (being D the set of points $\{(x, x)\} \subset \mathbb{R}^2$), $\|a - \gamma(a)\|_{\infty} = \max\{|x - x'|, |y - y'|\}$ and γ is a bijection that can associate a point off the diagonal with another point on or off the diagonal. Here, *diagonal* is the set D . Table 2 shows bottleneck distance between the persistence diagrams shown in Fig. 8.

The following definitions are taken from [2]. Let W and W' be the vertex set of, respectively, K and K' . A *correspondence* $C : W \Rightarrow W'$ from W to W' is a subset C of $W \times W'$ satisfying that for any $v \in W$ there exists $v' \in W'$ such that $(v, v') \in C$ and, conversely, for any $v' \in W'$ there exists $v \in W$ such that $(v, v') \in C$.

Besides, for a subset σ of W , $C(\sigma)$ is the subset of W' satisfying that a vertex v' is in $C(\sigma)$ if and only if there exists a vertex $v \in \sigma$ such that $(v, v') \in C$.

Now, given filter functions $f : K \rightarrow \mathbb{R}$ and $f' : K' \rightarrow \mathbb{R}$, and the corresponding filtrations F and F' , we say that $C : W \Rightarrow W'$ is ϵ -*simplicial* from F to F' if for any $t \in \mathbb{R}$ and simplex σ such that $f(\sigma) \leq t$, every simplex $\mu \in K'$ with vertices in $C(\sigma)$ satisfies that $f'(\mu) \leq t + \epsilon$.

Proposition 1 *If the correspondence $C : W \Rightarrow W'$ is ϵ -simplicial from F to F' , then $d_b(dgm(F), dgm(F')) \leq \epsilon$.*

Proof. The statement is a direct consequence of Th. 2.3 and Prop. 4.2 in [2]. \square

Proposition 2 *Let I (resp. I') be a 3D binary image. Let ∂K_{π} (resp. $\partial K'_{\pi}$) be the filtrations for $\partial K(I)$ (resp. $\partial K(I')$) associated to a given plane π . If $C : W \Rightarrow W'$ is a correspondence from the vertex set W of $\partial K(I)$*

to the vertex set W' of $\partial K(I')$ satisfying that $f_\pi(v') \leq f_\pi(v) + \epsilon$ for every $(v, v') \in C$, then

$$C : W \Rightarrow W' \text{ is } \epsilon\text{-simplicial from } \partial K_\pi \text{ to } \partial K'_\pi.$$

Proof. Let $t \in \mathbb{R}$ and $\sigma \in \partial K(I)$ such that $f_\pi(\sigma) \leq t$. Then, every simplex $\mu \in K'$ with vertices in $C(\sigma)$ satisfies that $f_\pi(\mu) \leq t + \epsilon$. Then, $C : W \Rightarrow W'$ is ϵ -simplicial from ∂K_π to $\partial K'_\pi$. \square

The following is the main result of the paper showing, in terms of probabilities, that the topological gait signature is stable under small perturbations on the input data (i.e., the input gait sequence).

Theorem 1 *Let I (resp. I') be a 3D binary image. Let ∂K_π (resp. $\partial K'_\pi$) be the filtration for $\partial K(I)$ (resp. $\partial K(I')$), associated to a given plane π . Let $\mathcal{V}_\pi^0, \mathcal{V}_\pi^1$ (resp. $\mathcal{W}_\pi^0, \mathcal{W}_\pi^1$) be the two vectors obtained after applying Proc. 1 to the persistence barcodes of ∂K_π (resp. $\partial K'_\pi$). Suppose that $m_i = m_i^{K_{\pi^i}}$ is less or equal than $m_i^{K'_{\pi^i}}$, where $m_i^{K_\pi}$ (resp. $m_i^{K'_\pi}$) is the number of bars in the i -persistence barcodes (for $i = 0, 1$) of the filtrations ∂K_π (resp. $\partial K'_\pi$). If $C : W \Rightarrow W'$ is a correspondence from the vertex set W of $\partial K(I)$ to the vertex set W' of $\partial K(I')$ satisfying that $f_\pi(v') \leq f_\pi(v) + \epsilon$ then*

$$\mathcal{V}_\pi^i = \mathcal{W}_\pi^i \text{ with probability greater or equal than } \left(1 - \frac{2(n-1)\epsilon}{k}\right)^{m_i}$$

where:

- k is the maximum distance of a point in ∂K_π to the plane π ;
- n is the number of subintervals (“windows”) in which the interval $[0, k]$ is divided (recall that we set $n = 24$ in our experiments);

In general, $\|\mathcal{V}_\pi^i - \mathcal{W}_\pi^i\|_1 \leq m$ with probability greater or equal than

$$P = \sum_{j=0}^m \binom{m_i}{j} \left(\frac{2(n-1)\epsilon}{k}\right)^j \left(1 - \frac{2(n-1)\epsilon}{k}\right)^{m_i-j}.$$

Observe that the result above only makes sense when ϵ is small enough. Concretely, $\epsilon \leq \frac{k}{2n}$ since $\frac{k}{2n}$ is half of the “window” size. Besides m can take integer values between 0 and m_i . Observe that if $m = 0$ then $P = \left(1 - \frac{2(n-1)\epsilon}{k}\right)^{m_i}$ and if $m = m_i$ then $P = 1$.

Proof. By Prop. 2, we have that $C : W \Rightarrow W'$ is ϵ -simplicial from ∂K_π to $\partial K'_\pi$. By Prop. 1, we have that $d_b(dgm(\partial K_\pi), dgm(\partial K'_\pi)) \leq \epsilon$.

Let $\gamma : dgm(\partial K_\pi) \cup \{(x, x)\} \rightarrow dgm(\partial K'_\pi) \cup \{(x, x)\}$ be the bijection such that $\{\max_a \{\|a - \gamma(a)\|_\infty\}\} = d_b(dgm(\partial K_\pi), dgm(\partial K'_\pi)) \leq \epsilon$. If $a = (x, y)$ and $\gamma(a) = (x', y')$, we have that $|x - x'| \leq \epsilon$ and $|y - y'| \leq \epsilon$.

Now, observe that \mathcal{V}_π^i can be different from \mathcal{W}_π^i if there exists a point $a =$

(x, y) in $dgm(\partial K_\pi)$ satisfying that $x \in (sh - \epsilon, sh + \epsilon)$ for $h = \lfloor \frac{k}{n} \rfloor$ and some $s = 1, \dots, n - 1$. This can occur with probability $\frac{2(n-1)\epsilon}{k}$. Then $\mathcal{V}_\pi^i = \mathcal{W}_\pi^i$ with probability greater or equal than $(1 - \frac{2(n-1)\epsilon}{k})^{m_i}$. \square

For example, if $k = 0.9$, $n = 24$, $\epsilon = 0.001$, $m_0 = 50$ and $m = 3$ then 0.7235226992 ; if $m = 4$ then $P = 0.8732685424$ and if $m = 5$ then $P = 0.9508832893$. This means that given two digital images I and I' and a plane π such that there exists a correspondence C between the vertices of $\partial K(I)$ and $\partial K(I')$ satisfying that $f_\pi(v') \leq f_\pi(v) + 0.001$ for any pair of vertices $v \in \partial K(I)$ and $v' \in \partial K(I')$ matched by C , then for the associated topological signatures \mathcal{V}_π^0 and \mathcal{W}_π^0 (for $k = 0.9$, $n = 24$ and $m_0 = 50$) we have that:

- $\|\mathcal{V}_\pi^0 - \mathcal{W}_\pi^0\|_1 \leq 3$ with probability greater or equal than 72%.
- $\|\mathcal{V}_\pi^0 - \mathcal{W}_\pi^0\|_1 \leq 4$ with probability greater or equal than 87%.
- $\|\mathcal{V}_\pi^0 - \mathcal{W}_\pi^0\|_1 \leq 5$ with probability greater or equal than 95%.

The following remark shows that the topological gait signature does not depend on the number of gait cycles in a gait sequence.

Remark 1 *In the case the gait sequence contains more than a gait cycle, the module of the vectors $\{\mathcal{V}_{\pi_i}^0, \mathcal{V}_{\pi_i}^1\}_{i=1, \dots, 8}$ can increase with respect to the gait sequence that contains exactly a gait cycle, but the direction remains the same.*

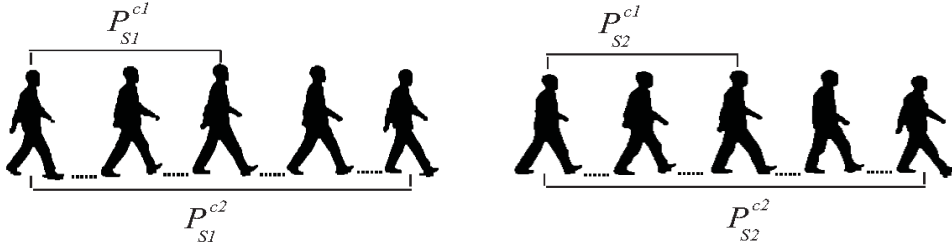


Figure 7: The silhouette sequences extracted from two gait sequences S_1 and S_2 of the same person.

For instance, let S_1 and S_2 be two gait sequences of the same person from CASIA-B dataset, both S_1 and S_2 having two gait cycles. Let $P_{s_1}^{c2}$ and $P_{s_2}^{c2}$ be the silhouette sequences of the two gait cycles on S_1 and S_2 , respectively. Let $P_{s_1}^{c1}$ and $P_{s_2}^{c1}$ be the silhouette sequences of exactly one gait cycle on S_1 and S_2 , respectively. See Fig. 7.

Then, we use the same reference plane π to obtain the four filtrations $F_{s_1}^{c2}$, $F_{s_2}^{c2}$, $F_{s_1}^{c1}$ and $F_{s_2}^{c1}$ for the simplicial complexes associated to the 3D binary images obtained from the silhouette sequences $P_{s_1}^{c2}$, $P_{s_2}^{c2}$, $P_{s_1}^{c1}$ and $P_{s_2}^{c1}$,

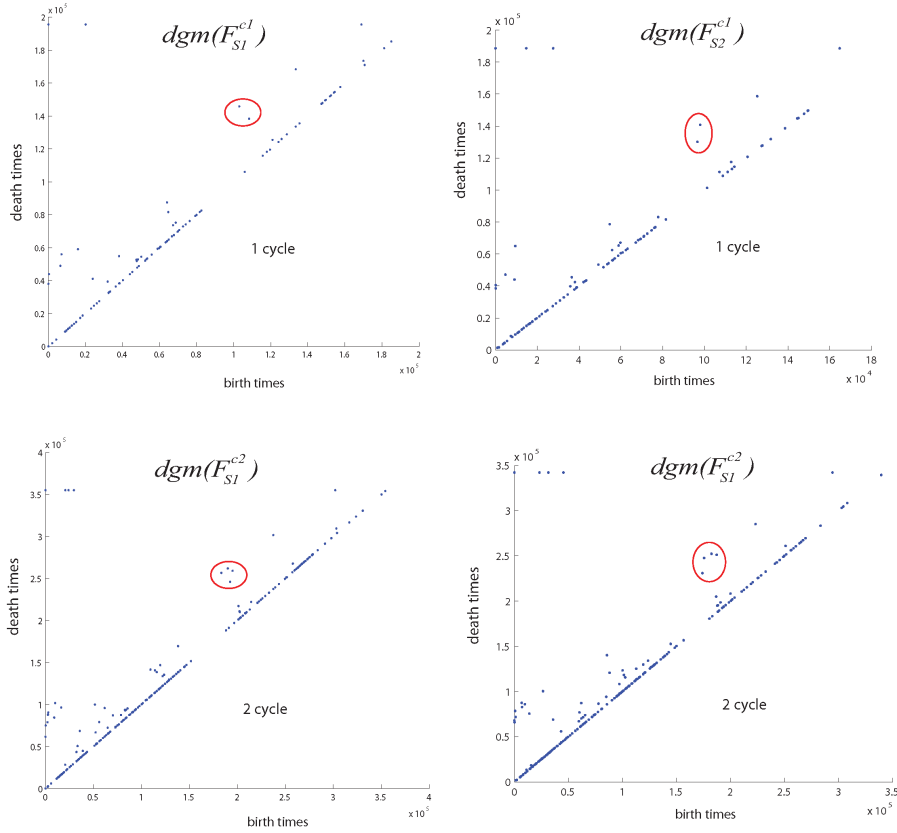


Figure 8: Top pictures: the two 0–persistence diagrams $dgm(F_{s1}^{c1})$ and $dgm(F_{s2}^{c1})$ obtained from two gait sequences of the same person containing exactly one gait cycle. Bottom pictures: the 0–persistence diagrams $dgm(F_{s1}^{c2})$ and $dgm(F_{s2}^{c2})$ obtained from two gait sequences of the same person containing two gait cycles.

respectively. The 0–persistence diagrams $dgm(F_{s1}^{c2})$, $dgm(F_{s2}^{c2})$, $dgm(F_{s1}^{c1})$ and $dgm(F_{s2}^{c1})$ are showed in Fig. 8. We can observe that the diagrams $dgm(F_{s1}^{c2})$ and $dgm(F_{s2}^{c2})$ have the double of persistent points than the diagrams $dgm(F_{s1}^{c1})$ and $dgm(F_{s2}^{c1})$ (look at the area inside of the red circles in Fig. 8). Since the topological gait signature is computed using “windows” in the persistence barcode (or equivalent, in the persistence diagram), then the modules of the gait signature of $dgm(F_{s1}^{c2})$ and $dgm(F_{s2}^{c2})$ is approximately the double of the modules of the gait signature of $dgm(F_{s1}^{c1})$ and $dgm(F_{s2}^{c1})$ but the direction remains the same.

In Table 1 we show the results of the comparison between the topological signatures obtained from the diagrams $dgm(F_{s1}^{c2})$, $dgm(F_{s2}^{c2})$, $dgm(F_{s1}^{c1})$ and $dgm(F_{s2}^{c1})$ using the cosine distance. Observe that, in all cases, the cosine distance is almost 1 (i.e., all the vectors have almost the same direction),

which makes sense since all the gait sequences correspond to the same person and the corresponding filtrations are computed using the same reference plane.

Table 1: Cosine distance between persistence diagrams according to Fig. 8.

	$dgm(F_{S_2}^{c1})$	$dgm(F_{S_2}^{c2})$
$dgm(F_{S_1}^{c1})$	0.985	0.987
$dgm(F_{S_1}^{c2})$	0.981	0.990

Finally, in Table 2 we show that if we consider the classical bottleneck distance for comparing the different persistence diagrams, we obtain different results depending on the number of gait cycles we consider to compute the gait signature. So, the comparison using bottleneck distance does not provide useful information in this case.

Table 2: Bottleneck distance between persistence diagrams according to Fig. 8.

	$dgm(F_{S_2}^{c1})$	$dgm(F_{S_2}^{c2})$
$dgm(F_{S_1}^{c1})$	855727	1319872
$dgm(F_{S_1}^{c2})$	2273559	5446584

We now repeat the experiment for gait sequences obtained from two different persons and **considering only the lowest fourth part of the body silhouettes**. Let $001 - nm1$ and $001 - nm2$ be two gait sequences of the person 001 and $008 - nm2$ a gait sequence of person 008 taken from CASIA-B dataset.

Let $\partial K(I_{001-nm1}^{ci})$, $\partial K(I_{001-nm2}^{ci})$ and $\partial K(I_{008-nm2}^{ci})$ be the simplicial complexes associated to the silhouettes sequences of exactly i gait cycles on $001 - nm1$, $001 - nm2$ and $008 - nm2$, for $i = 1, 2$.

A fixed reference plane π is used to obtain the 0-persistence diagrams $dgm(F_{001-nm1}^{ci})$, $dgm(F_{001-nm2}^{ci})$, $dgm(F_{008-nm2}^{ci})$ of the simplicial complex associated to $\partial K(I_{001-nm1}^{ci})$, $\partial K(I_{001-nm2}^{ci})$ and $\partial K(I_{008-nm2}^{ci})$, respectively (see Fig. 9). Observe in Fig. 9 that the persistence diagrams obtained from two gait cycles have the double of persistent points than the persistence diagrams obtained from one gait cycle. This can be noticed in the area inside of the red circles in Fig. 9.

In Table 3 and Table 4 we show the results for the comparison between the topological signatures obtained from the previously computed persistence diagrams, using bottleneck and cosine distance, respectively.

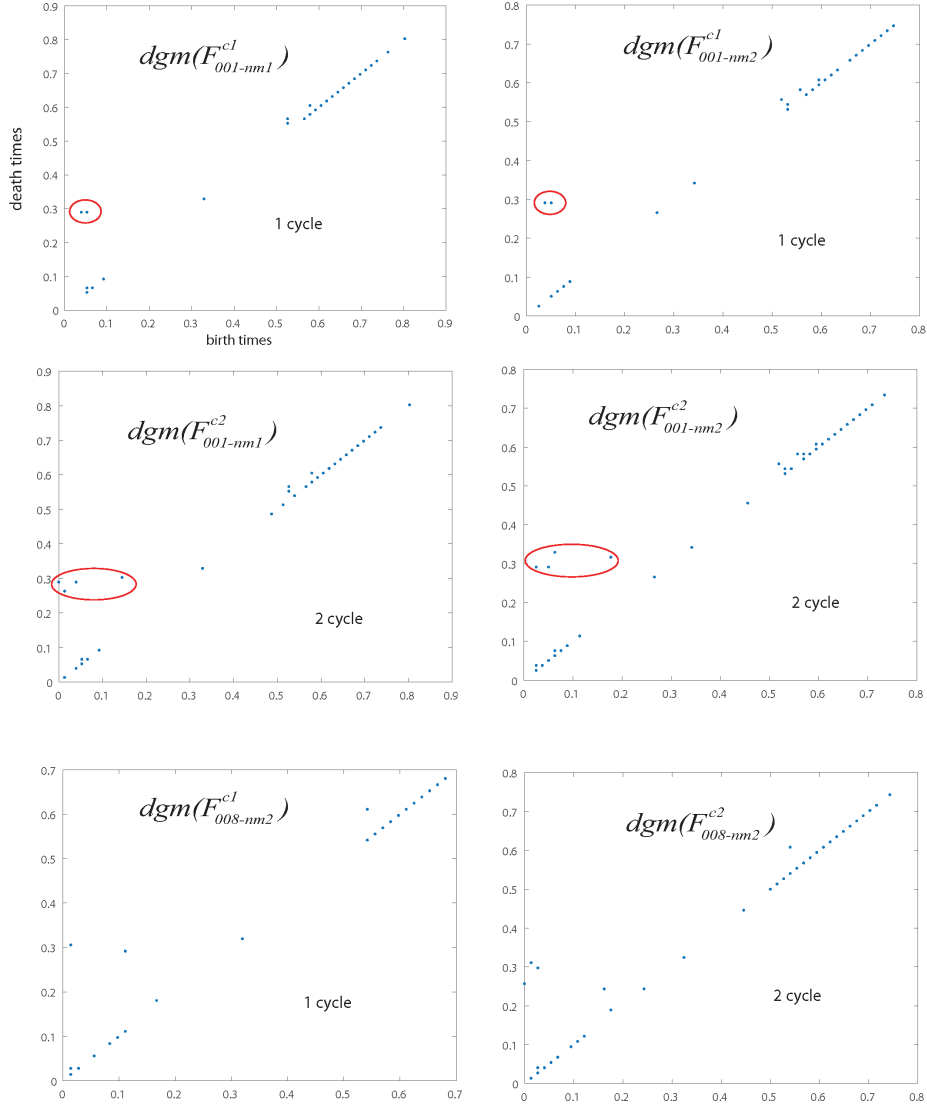


Figure 9: On top, the two 0–persistence diagrams $dgm(F_{001-nm1}^{c1})$, $dgm(F_{001-nm2}^{c1})$. In the middle, the two 0–persistence diagrams $dgm(F_{001-nm1}^{c2})$, $dgm(F_{001-nm2}^{c2})$. On bottom, the two 0–persistence diagrams $dgm(F_{008-nm1}^{c1})$, $dgm(F_{008-nm2}^{c2})$.

The results show that the value of the bottleneck distance increases with the number of gait cycles. However, the values are similar when the cosine distance is used. Furthermore, the comparative between diagrams with two cycles, which mean more information of the dynamic of gait, could improve the similarity, i.e, the bottleneck distance decreases and the cosine distance is closer to one.

The tables show that the cosine distance is more appropriate than bot-

Table 3: Bottleneck distance between persistence diagrams according to Fig. 8.

	$dgm(F_{001-nm2}^{c1})$	$dgm(F_{001-nm2}^{c2})$	$dgm(F_{008-nm2}^{c1})$	$dgm(F_{008-nm2}^{c2})$
$dgm(F_{001-nm1}^{c1})$	0.013	0.120	0.06	0.128
$dgm(F_{001-nm1}^{c2})$	0.125	0.040	0.125	0.059

Table 4: Cosine distance between the persistence diagrams showed in Fig. 9.

	$dgm(F_{001-nm2}^{c1})$	$dgm(F_{001-nm2}^{c2})$	$dgm(F_{008-nm2}^{c1})$	$dgm(F_{008-nm2}^{c2})$
$dgm(F_{001-nm1}^{c1})$	0.944	0.931	0.739	0.886
$dgm(F_{001-nm1}^{c2})$	0.929	0.953	0.832	0.905

tleneck distance to compare gait signatures.

5 Experimental Results

In this section we show the accuracy results in two experiments using CASIA-B dataset. The CASIA-B dataset has 124 persons, and 10 samples for each of the 11 different angles at which a person is taken. For each angle there are six samples walking under natural conditions, which means without carrying a bag or wearing a coat (CASIA-Bnm), there are two samples of persons carrying some sort of bag (CASIA-Bbg) and the remaining two samples for persons wearing coat (CASIA-Bcl). CASIA-B dataset provides image sequences with background segmentation for each person.

In the first experiment we used four sequences by person from CASIA-Bnm dataset to train. We used the other two sequences by person from CASIA-Bnm and the sequences from CASIA-Bbg and CASIA-Bcl to test. Our results for lateral view (90 degrees) are shown in Table 5, where we take the cross validation average ($\binom{6}{4} = 15$ combinations) of accuracy at rank 1 from the candidates list. The result of our previous method [10] was also evaluated using always the lowest fourth part of the body silhouette.

In the second experiment, we followed the protocol used in [1, Section 5.3]. This way, we considered a mixture of normal, carrying-bag and wearing-coat sequences, since it models a more realistic situation where persons do not collaborate while the samples are being taken. Specifically, six sequences were used to training (four normal sequences, one carrying-bag sequence and one wearing-coat sequence), the rest was used to test. Table 6 shows the result of the accuracy.

Table 5: Accuracy (in %) using training sets consisting of samples under similar covariate conditions (without carrying a bag or wearing a coat).

Methods	CASIA-Bbg	CASIA-Bcl	CASIA-Bnm	Average
Tieniu.T [17]	52.0	32.73	97.6	60.8
Khalid.B [1]	78.3	44.0	100	74.1
Singh.S [15]	74.58	77.04	93.44	81.7
Imad.R et al. [14]	81.70	68.80	93.60	81.40
Lishani et al. [12]	76.90	83.30	88.70	83.00
Previous Method [10]	75.8	75.45	90.3	80.5
Our Method				
using cosine	80.5	81.7	92.4	84.9
using angle	84.2	87.6	94.1	88.6

Table 6: Accuracy (in %) using training sets consisting of samples under different covariate conditions (walking-normal, carrying-bag and wearing-coat).

Methods	CASIA-Bbg	CASIA-Bcl	CASIA-Bnm	Average
Khalid.B [1]	55.6	34.7	69.1	53.1
Our Method	92.3	94.3	94.7	93.8

A third experiment was carried out for obtaining Fig. 10. In this case six sequences were used for training (one with the person carrying a bag, one with the person wearing a coat and four with the person walking under natural conditions). Using this training data we generated 123 topological signatures, one for each person in the database. We used the remaining sequence of the person carrying a bag and the one wearing a coat for testing. This gave us 246 sequences for testing: 123 persons times 2 sequences by person. We must point out that person labeled as 005 in CAISA-B was removed from the experiment due to poor quality.

Using the obtained topological signatures and testing set we obtained:

- (1) The set of all possible comparisons between the obtained signatures and the signatures of the test sequences, corresponding to the same person. This set is called True Positive (TP) and contains 246 comparison values.
- (2) The set of all possible comparisons between the obtained signatures and the signatures of the test sequences, corresponding to different persons. This set is called True Negative (TN) and contains $123 \times 244 = 30012$ values.

For obtaining Fig. 10, we first restricted TN to its 246 smallest values, in order to balance the sets TP and TN. Then we represented in the y axis

the percent of values in the TP set lower than a threshold as a red curve and the same for the TN set as a blue curve. The x axis represents all the considered thresholds. For example, 92.6% of the data in the set TP are values smaller than 253.8, since the red curve shows that for $x = 253.8$ we have that $y = 92.6\%$.

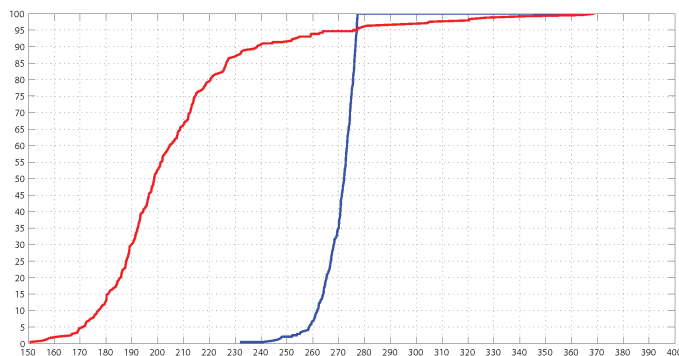


Figure 10: Result of the comparison between the training set and the test set for the topological signatures of the sequences representing the same person (in red) and the one between the training set and the test set for the topological signatures of the sequences representing different persons (in blue).

More examples and the source code written in Matlab can be obtained visiting the web page: <http://grupo.us.es/cimagroup/>.

6 Analysis of the results

In Table 5 we see that the best result of our method was for the set of normal sequences (CASIA-Bnm) and the worst was for the set of persons carrying bags. This is due to that bags can affect the accuracy of the method (see the lowest fourth part of the body silhouette in Fig. 1). Moreover, the weight of the bag can change the dynamic of the gait. On the other hand, the features obtained from the lowest fourth part of the body silhouette gave an accuracy for the normal sequences of 94.1%, which only decreases 3.9% with respect to our previous paper [10] using the whole body silhouette (98.0%). This confirms that the highest information in the gait is in the motion of the legs, which supports the results given in [1].

Nevertheless, as we can see in Tables 5 and 6, our method outperforms previous methods for gait recognition with or without carrying a bag or wearing a coat. Furthermore, we show in Table 5 that the changes introduced to obtain our new method derive in an improvement with respect to our previous solution [10].

Besides, the algorithm explained in [1] decreases considerably the accu-

racy obtained by training mixing the normal, carrying-bag and wearing-coat sequences (see Table 6). On the contrary, our algorithm improves the accuracy for the whole test set. Comparing the two tables, we can as well arrive to the conclusion that training with more heterogeneous data gives to our method a more powerful representation for the classification step and in that case, our method outperforms in more than 35% the results given in [1].

Finally, the results presented in this paper show the power of the Theory of Persistent Homology to obtain the structural features of the dynamic of the legs.

7 Conclusion

In this paper we have presented an algorithm for gait recognition, a technique with special attention in tasks of video surveillance. We have used persistent homology to model the gait, similar as we did in our previous approaches, although the algorithm presented here is slightly different to our previous ones in a way that it is more robust to variations in the amount of simplices considered and removes as well any dependency with respect to the stability of the sorting algorithm used for obtaining the filtration. Besides, the topological features have been tested here using only the lowest fourth part of the body silhouette. Then, the effects of variations unrelated to the gait in the upper body part, which are very frequent in real scenarios, decrease considerably. We have proved that our topological signature is robust to small perturbations in the input data and does not depend on the number of gait cycles contained in the gait sequence. Finally, the results presented in the paper improve considerably the accuracy in the state of the art.

Acknowledgments

This work has been partially supported by IMUS and MINECO/FEDER-UE under grant MTM2015-67072-P.

References

- [1] Bashir, K., Xiang, T., Gong, S.: Gait recognition without subject cooperation. *Pattern Recognition Letters* 31(13), 20522060 (2010)
- [2] Chazal, F., de Silva, V., Oudot, S.: Persistence stability for geometric complexes. *Geometriae Dedicata* 173(1), 193214 (2014)

- [3] Chen, C., Liang, J., Zhao, H., Hu, H., Tian, J.: Frame difference energy image for gait recognition with incomplete silhouettes. *Pattern Recognition Letters* 30(11), 977984 (2009)
- [4] Edelsbrunner, H., Harer, J.: *Computational topology: an introduction*. American Mathematical Soc. (2010)
- [5] Ghrist, R.: Barcodes: The persistent topology of data. *Bull. Amer. Math. Soc.* 45 (2008), 61-75 45, 6175 (2008)
- [6] Lamar-Leon, J., Alonso-Baryolo, R., Garcia-Reyes, E., Gonzalez-Diaz, R.: Gait-based carried object detection using persistent homology. In: *Progress in Pattern Recognition, Image Analysis, Computer Vision, and Applications - 19th Iberoamerican Congress, CIARP 2014, Puerto Vallarta, Mexico, November 2-5, 2014. Proceedings*, pp. 836843 (2014)
- [7] Lamar-Leon, J., Alonso-Baryolo, R., Garcia-Reyes, E., Gonzalez-Diaz, R.: Topological features for monitoring human activities at distance. In: *Activity Monitoring by Multiple Distributed Sensing - Second International Workshop, AMMDS 2014, Stockholm, Sweden, August 24, 2014*, pp. 4051 (2014)
- [8] Lamar-Leon, J., Baryolo, R.A., Garcia-Reyes, E., Gonzalez-Diaz, R.: Persistent homology-based gait recognition robust to upper body variations. In: *23rd International Conference on Pattern Recognition, ICPR 2016, Cancun, Mexico, December 4-8, 2016*, pp. 10831088 (2016)
- [9] Lamar-Leon, J., Cerri, A., Garcia-Reyes, E., Gonzalez-Diaz, R.: Gait-based gender classification using persistent homology. In: *Progress in Pattern Recognition, Image Analysis, Computer Vision, and Applications - 18th Iberoamerican Congress, CIARP 2013, Havana, Cuba, November 20-23, 2013, Proceedings, Part II*, pp. 366373 (2013)
- [10] Lamar-Leon, J., Garcia-Reyes, E., Gonzalez-Diaz, R.: Human gait identification using persistent homology. In: *Progress in Pattern Recognition, Image Analysis, Computer Vision, and Applications - 17th Iberoamerican Congress, CIARP 2012, Buenos Aires, Argentina, September 3-6, 2012. Proceedings*, pp. 244251 (2012)
- [11] Lee, C.P., Tan, A.W., Tan, S.C.: Time-sliced averaged motion history image for gait recognition. *Journal of Visual Communication and Image Representation* 25(5), 822 826 (2014)
- [12] Lishani, A.O., Boubchir, L., Bouridane, A.: Haralick features for gait-based human gait recognition. In: *Microelectronics (ICM), 2014 26th International Conference on*, pp. 3639. IEEE (2014)

- [13] Munkres, J.R.: Elements of algebraic topology, vol. 2. Addison-Wesley Reading (1984)
- [14] Rida, I., Almaadeed, S., Bouridane, A.: Gait recognition based on modified phase-only correlation. *Signal, Image and Video Processing* 10(3), 463470 (2016)
- [15] Singh, S., Biswas, K.: Biometric gait recognition with carrying and clothing variants. In: *Pattern Recognition and Machine Intelligence*, pp. 446451. Springer (2009)
- [16] Wu, Z., Huang, Y., Wang, L., Wang, X., Tan, T.: A comprehensive study on cross-view gait based human identification with deep cnns. *IEEE transactions on pattern analysis and machine intelligence* 39(2), 209226 (2017)
- [17] Yu, S., Tan, D., Tan, T.: A framework for evaluating the effect of view angle, clothing and carrying condition on gait recognition. In: *Pattern Recognition, 2006. ICPR 2006. 18th International Conference on*, vol. 4, pp. 441444. IEEE (2006)
- [18] Zhang, Y., Jiang, S., Yang, Z., Zhao, Y., Guo, T.: A score level fusion framework for gait-based human recognition. In: *Multimedia Signal Processing (MMSP), 2013 IEEE 15th International Workshop on*, pp. 189194. IEEE (2013)